43rd AIAA Aerospace Sciences Meeting and Exhibit, 10-13 January 2005, Reno, Nevada

Accurate Estimates of Fine Scale Reaction Zone Thicknesses in Gas Phase Detonations

Joseph M. Powers* and Samuel Paolucci†

University of Notre Dame, Notre Dame, Indiana, 46556-5637, USA

A robust method is developed and used to provide rational estimates of reaction zone thicknesses in one-dimensional steady gas phase detonations in mixtures of inviscid ideal reacting gases whose chemistry is described by detailed kinetics of the interactions of N molecular species constituted from L atomic elements. The conservation principles are cast as a set of algebraic relations giving pressure, temperature, density, velocity, and L species mass fractions as functions of the remaining $N-L$ species mass fractions. These are used to recast the $N-L$ species evolution equations as a self-contained system of non-linear ordinary differential equations of the form $dY_i/dx = f_i(Y_1, \ldots, Y_{N-L})$. These equations are numerically integrated from a shock to an equilibrium end state. The eigenvalues of the Jacobian of f_i are calculated at every point in space, and their reciprocals give local estimates of all length scales. Application of the method to the standard problem of a stoichiometric Chapman-Jouguet hydrogen-air detonation in a mixture with ambient pressure of $1\ atm$ and temperature of $298\ K$ reveals that the finest length scale is on the order of $10^{-5}\ cm$; this is orders of magnitude smaller than both the induction zone length, $10^{-2}\ cm$, and the overall reaction zone length, $10^{0}\ cm$. In order to achieve numerical stability and convergence of the solution at a rate consistent with the order of accuracy of the numerical method as the spatial grid is refined, it is shown that one must employ a grid with a finer spatial discretization than the smallest physical length scale.

I. Introduction

In recent years there has been great interest in computations of complex multi-scale physical phenomena. In this work, the simple issue of whether such computations have captured the breadth of length scales they purport to model is examined, and conditions are found under which such predictions are mathematically verifiable. The specific purpose of this paper is to give an accurate estimate of what spatial resolution is necessary for an important paradigm multi-scale problem: gas phase detonation described by detailed chemical kinetics. The general approach presented here can be extended to a wider range of problems, including those that are the subject of present intense computational investigations such as laminar flame propagation, supernovæ dynamics, combustion in reactive solids, flows in jet engines, and flows in rocket nozzles.

The ever-increasing capabilities of computational hardware and algorithms offer the scientific and engineering communities the opportunity to solve unsteady multi-dimensional problems which only a few years ago would have been impossible. However, this has necessitated a more complex interplay between mathematics, computation, and experiment; in order to determine via computation whether the underlying mathematical model is representative of the observable physics, one must first guarantee that the computations have fidelity with the underlying mathematics; this is sometimes defined as verification. Only then is it appropriate to make comparisons with experiment, sometimes defined as validation, which, while critically important, will not be considered here. Neglecting the process of harmonizing computational predictions with the underlying mathematics, and thus simply tuning computational results with experiments, gives rise to the strong possibility that the predictions depend on both the size of the discrete grid and the particular algorithm used to solve the underlying equations.

*Associate Professor, AIAA Associate Fellow, powers@nd.edu.

†Professor, paolucci@nd.edu.

Concerns regarding verification are typically minimal in problems for which the spatial and temporal scales over which the system evolves are nearly the same order of magnitude. In such cases, errors are usually obvious and easily corrected. However, in so-called multi-scale problems, in which the range of spatio-temporal scales may span many orders of magnitude, verification is more difficult. In scenarios where the coupling across scales is weak, large scale results, readily seen in predictions, may be relatively insensitive to errors at the small scales. In other problems, typically with stronger non-linearities, the coupling across scales can be significant, and errors at the small scale can rapidly cascade to the large scale. Since for many problems it is difficult to obtain clear *a priori* information of the strength of this coupling, the only way one can gain confidence in predictions is to guarantee that all scales have been properly captured.

A prototypical multi-scale example is found in gas phase detonation with detailed chemistry. Over the past decades, the aerospace propulsion community has utilized multi-scale aerothermochemistry models of increasing complexity for sophisticated problems including flows in and around re-entry vehicles, rocket nozzles, supersonic combustion ramjets, and pulse detonation wave engines. As the geometries of these devices are on typical engineering scales and the chemistry typically evolves on a variety of significantly smaller length scales, it is clear that this is a multi-scale problem. It must be said that in some problems, such as determination of detonation wave speeds and peak pressures, *a posteriori* calculations reveal only a weak dependence on properly capturing fine scale structures. However, other calculations, for instance those of detonation instability or pollutant formation, can have a strong dependence on the fine structures. Whatever the case, it is not clear that the finest length scales have been resolved in most studies. Even in the most careful, it is rare to see a rigorous grid convergence study or an analysis which shows that the finest scales have been captured. To the contrary, it is more common to find the curious situation in which an argument is made for the necessity of a detailed kinetics model to capture the true physics of a problem, only to be followed by either 1) a rationalization as to why it is not necessary to have a fine grid capture the detailed physics, or more commonly, 2) no recognition that fine scale physics has been overwhelmed by numerical errors.

To highlight this point, this study focuses on one key issue: determination of the finest length scale necessary to capture the smallest features present in a routinely-used aerothermochemistry model of detonation. If calculations based on models of this class are to be able to withstand scientific scrutiny with regards to repeatability, grid- and algorithm-independence, consistent with AIAA standards for computations, they must, at a minimum, capture this finest scale. Even then, depending on the problem, there may be even finer length scales present, due to other effects, *e.g.* high wavenumber instabilities or multidimensionality.

This study considers the issue of length scales by addressing a single paradigm problem: a one-dimensional steady Chapman-Jouguet (CJ) detonation in an inviscid stoichiometric hydrogen-air mixture whose chemistry is described by nine species undergoing nineteen reversible reactions. While there is often controversy regarding parameter values in detailed kinetics models, especially for high molecular weight hydrocarbons, the detailed model for hydrogen oxidation is widely regarded as well understood, and parametric uncertainties are small.[1,2]

Initially, the mixture is taken to consist of diatomic hydrogen, oxygen, and nitrogen in the molar ratio of $2H_2 + O_2 + 3.76N_2$ at a pressure of 1 atm and temperature of 298 K. Nitrogen is modeled as an inert diluent. This is precisely the hydrogen-air problem studied by Shepherd[3], who reported global reaction zone structures. It is closely related to the study of Mikolaitis[4], who, following a general procedure used by Westbrook[2], used the same kinetics model to give one of the most carefully resolved calculations of the time variation of all variables within what is known as the induction zone, *i.e.* the early part of the reaction process in which pressure, temperature, and velocity are essentially constant and minor species mass fractions are rapidly growing. Shepherd's predictions of the variation of variables within the induction zone, while likely resolved, are difficult to discern in his plots. It will also be possible to compare to the recent results of Lu, *et al.*[5], who use a similar kinetics model to carefully predict induction zone lengths; however, they do not report the fine scale details. In a somewhat similar calculation, Fickett and Davis[1] give a fully resolved prediction of a steady CJ detonation in $2H_2 + O_2 + 9Ar$ initially at 300 K and 0.1 atm; as the ambient pressure is lower, the reaction zone is larger.

Of those spatio-temporal studies that exercise care in resolving spatial structures, it is typically the induction zone length which is deemed to be the smallest length scale to be resolved. Such is the case in the studies of Oran, *et al.*[6], Eckett, *et al.*[7], Pintgen, *et al.*[8], Sheffer, *et al.*[9,10], and Tsuboi, *et al.*[11] Nevertheless, as the thermal explosion at the end of the induction zone is the result of the cumulative non-linear effects of reactions at finer scales, it is natural to suppose accurate prediction of the induction zone depends on

accurate calculation of more primitive finer scale phenomena. The study of Singh, *et al.*[12] resolved the induction length scale as well as the finer viscous scale. Their calculations, which took advantage of an adaptive spatial discretization method, came closest to resolving the finest reaction scales. Other studies have been less rigorous and give predictions in which it is unclear if even the induction zone has been resolved. Examples include those of Fedkiw, *et al.*[13], Ebrahimi and Merkle[14], and Dudebout, *et al.*[15] Recognizing the difficulties in resolving the finest scales of detailed kinetics, others take alternate approaches: : 1) one-step kinetics, *cf.* He and Karagozian[16], or 2) two-step kinetics, *cf.* Sichel, *et al.*[17], or Kawai and Fujiwara[18], based on the approach of Korobeinikov, *et al.*[19]. Both one- and two-step models require some compromises, described fully by the cited authors, in which the sacrifice of many terms results in a restricted ability to describe some physical phenomena relative to the detailed models. Moreover, even in two-step studies, the relative lengths of the individual reaction zone structures are not always clarified; if the smallest is not resolved, the same concerns one has for detailed kinetics models are realized. That is to say, a small number of reactions in no way guarantees the computation is easy to perform accurately. In contrast, one could also have a system with hundreds of reactions, and if by chance they all evolved over a similar length scale, the computation could be done with both accuracy and efficiency.

The paper is organized as follows. First, a full description of the underlying unsteady reactive Euler equations is given. This is followed by details of the steps necessary to reduce the system to a set of ordinary differential equations (ODEs) describing the spatial evolution of a subset of the species mass fractions. Next, a standard linear analysis is performed to reveal that at a given point in the reaction zone structure, the local length scales over which the system evolves are given by the reciprocal of each of the eigenvalues of the local Jacobian matrix of the non-linear function on the right-hand side of the ODEs. This is followed by a description of the numerical method used to solve the system. Results are then shown for the spatial evolution of species mole fractions (used so that proper comparisons can be made with results in the literature), thermodynamic variables, and local length scales for the paradigm CJ detonation. A comparison of the finest scales to the induction zone length scales is given, followed by a numerical study of accuracy and stability. Then a summary of some recent predictions given in the literature of hydrogen-air, hydrogen-oxygen, and hydrogen-oxygen-argon detonations with detailed kinetics is given, and grid sizes used in those models are compared with the minimum physical length scale predicted by the present analysis. The implications of the results are reviewed in the concluding section.

II. Mathematical Model

A. Governing Equations

The following equations, written in unsteady conservative form, describe the behavior of a one-dimensional inviscid mixture of N gaseous molecular species composed of L atomic elements which undergo J reactions:

$$\frac{\partial \rho}{\partial t} + \frac{\partial}{\partial x}\left(\rho u\right) = 0, \tag{1}$$

$$\frac{\partial}{\partial t}\left(\rho u\right) + \frac{\partial}{\partial x}\left(\rho u^2 + p\right) = 0, \tag{2}$$

$$\frac{\partial}{\partial t}\left(\rho\left(e + \frac{u^2}{2}\right)\right) + \frac{\partial}{\partial x}\left(\rho u\left(e + \frac{u^2}{2} + \frac{p}{\rho}\right)\right) = 0, \tag{3}$$

$$\frac{\partial}{\partial t}\left(\rho Y_i\right) + \frac{\partial}{\partial x}\left(\rho u Y_i\right) = \dot{\omega}_i M_i, \qquad (i = 1, \ldots, N-1). \tag{4}$$

The independent variables are the distance coordinate, x, and time, t. The dependent variables are density, ρ, velocity u, pressure, p, specific internal energy e, species mass fractions $Y_i, i = 1, \ldots, N-1$, and molar production rate per unit volume for species i, $\dot{\omega}_i, i = 1, \ldots, N-1$. Equations (1-3) describe the conservation of mixture mass, linear momenta, and energy, respectively. Equation (4) describes the evolution of $N-1$ of the molecular species mass fractions.

The system is completed by the following algebraic equations:

$$p = \rho \Re T \sum_{i=1}^{N} \frac{Y_i}{M_i}, \tag{5}$$

$$e = \sum_{i=1}^{N} Y_i \left(h_i^{ref} + \int_{T_{ref}}^{T} c_{pi}(\hat{T}) d\hat{T} - \frac{\Re T}{M_i} \right), \tag{6}$$

$$1 = \sum_{i=1}^{N} Y_i, \tag{7}$$

$$\dot{\omega}_i = \sum_{j=1}^{J} r_j \left(\nu''_{ij} - \nu'_{ij} \right), \quad (i = 1, \ldots, N-1). \tag{8}$$

$$r_j = A_j T^{\beta_j} \exp\left(\frac{-E_j}{\Re T} \right) \left(\underbrace{\prod_{k=1}^{N} \left(\frac{\rho Y_k}{M_k} \right)^{\nu'_{kj}}}_{\text{forward}} - \underbrace{\frac{1}{K_j^c} \prod_{k=1}^{N} \left(\frac{\rho Y_k}{M_k} \right)^{\nu''_{kj}}}_{\text{reverse}} \right), \qquad (j = 1, \ldots, J), \tag{9}$$

$$K_j^c = \left(\frac{p^{ref}}{\Re T} \right)^{\sum_{m=1}^{N} \left(\nu''_{mj} - \nu'_{mj} \right)} \exp\left(\sum_{m=1}^{N} - \left(\nu''_{mj} - \nu'_{mj} \right) \frac{M_m g_m^{ref}}{\Re T} \right), (j = 1, \ldots, J), \tag{10}$$

$$M_i = \sum_{l=1}^{L} \phi_{il} m_l, \qquad (i = 1, \ldots, N), \tag{11}$$

$$\sum_{i=1}^{N} \nu'_{ij} \phi_{il} = \sum_{i=1}^{N} \nu''_{ij} \phi_{il}, \qquad (j = 1, \ldots, J), \ (l = 1, \ldots, L). \tag{12}$$

New dependent variables are the temperature, T, the specific heat at constant pressure of the i^{th} species, c_{pi}, taken to be a function of temperature, where $\hat{T}$ is a dummy variable of integration, the mass fraction of the N^{th} species, Y_N, the reaction rate of the j^{th} reaction, r_j, and the so-called equilibrium "constant" of the j^{th} reaction K_j^c. Parameters in Eqs. (5-12) are as follows. The universal gas constant is $\Re$. The pressure at the reference state is p^{ref}. For each molecular species from $i = 1, \ldots, N$, one has molecular mass, M_i, and reference state specific Gibbs free energy, g_i^{ref}. For each reaction $j = 1, \ldots, J$, one has frequency factor A_j, exponent characterizing power-law temperature dependency, β_j, activation energy E_j, and stoichiometric coefficients denoting the number of moles of reactant and product, respectively, of species i in reaction j, ν'_{ij}, ν''_{ij}. For $l = 1, \ldots, L$, the atomic element mass is m_l. For species $i = 1, \ldots, N$, and atomic element $l = 1, \ldots, L$, the species atomic element index giving number of moles of atomic element l in species i is ϕ_{il}. Equation (5) is a thermal equation of state for a mixture of ideal gases which obeys Dalton's law. Equation (6) is the corresponding caloric equation of state. Equation (7) constrains the species mass fractions to sum to unity. Equation (8) is an expression for the molar species evolution rate per unit volume for species i. Equation (9) is an expression of the law of mass action with Arrhenius kinetics for reaction j constructed so as to insure the forward and reverse reaction rate components satisfy Le Châtlier's principle as each individual reaction approaches equilibrium. Equation (10) is an equation for the equilibrium "constant" for each reaction. Equation (11) defines the molecular mass in terms of its constitutive atomic elements. Equation (12) is a stoichiometric constraint on atomic element l in reaction j. After use of Eqs. (8-10) to eliminate $\dot{\omega}_i$ in Eq. (4), Eqs. (1-7) form $5 + N$ equations in the $5 + N$ unknowns, ρ, u, p, e, T, $Y_i, \ldots, Y_N$.

A non-obvious identity is obtained by operating on the N-term version of Eq. (4). One notes that by summing Eq. (4) from $i = 1$ to N and employing Eqs. (8, 11-12), one arrives at

$$\frac{\partial}{\partial t} \left(\rho \sum_{i=1}^{N} Y_i \right) + \frac{\partial}{\partial x} \left(\rho u \sum_{i=1}^{N} Y_i \right) = \sum_{j=1}^{J} r_j \sum_{l=1}^{L} m_l \underbrace{\sum_{i=1}^{N} \phi_{il} \left(\nu''_{ij} - \nu'_{ij} \right)}_{=0} = 0. \tag{13}$$

Using next Eq. (7) to eliminate the sum of mass fractions in Eq. (13), one finds consistency with Eq. (1).

Additional useful auxiliary equations are as follows:

$$y_l = m_l \sum_{i=1}^{N} \frac{\phi_{il}}{M_i} Y_i, \qquad (l = 1, \ldots L), \tag{14}$$

$$X_i = \frac{\frac{Y_i}{M_i}}{\sum_{j=1}^{N} \frac{Y_j}{M_j}}, \qquad (i = 1, \ldots, N), \tag{15}$$

$$c_{vi} = c_{pi} - \frac{\Re}{M_i}, \qquad (i = 1, \ldots, N), \tag{16}$$

$$c_p = \sum_{i=1}^{N} Y_i c_{pi}, \tag{17}$$

$$c_v = \sum_{i=1}^{N} Y_i c_{vi}, \tag{18}$$

$$\gamma = \frac{c_p}{c_v}, \tag{19}$$

$$c = \sqrt{\gamma \frac{p}{\rho}}, \tag{20}$$

$$M = \frac{u}{c}, \tag{21}$$

$$p_i = \rho \Re \frac{Y_i}{M_i}, \tag{22}$$

$$\mu_i = M_i g_i^{ref} + \Re T \ln\left(\frac{p_i}{p^{ref}}\right), \tag{23}$$

$$1 = \sum_{l=1}^{L} y_l. \tag{24}$$

New dependent variables in Eqs. (14-24) are as follows. For each atomic element $l = 1, \ldots, L$, one has the element mass fraction, y_l. For each molecular species, $i = 1, \ldots, N$, one has the mole fraction, X_i, the specific heat at constant volume, c_{vi}, the partial pressure p_i, and the chemical potential μ_i. One has the mass-averaged specific heats at constant pressure and volume, respectively, c_p, c_v, the ratio of specific heats, γ, the frozen acoustic speed, c, and the Mach number, M. Equations (14-21) are definitions of y_l, X_i, c_{vi}, c_p, c_v, γ, c, M, p_i, and μ_i, respectively. Lastly, Eq. (24) constrains the atomic element mass fractions and can be derived from summing Eq. (14) from $l = 1$ to L and employing Eq. (11).

It is easily shown that Eqs. (1-7) form a hyperbolic system, and thus admit propagating discontinuous jumps. For a stationary jump, which will be considered here, the equations reduce to

$$[\![\rho u]\!] = 0, \tag{25}$$

$$[\![\rho u^2 + p]\!] = 0, \tag{26}$$

$$\left[\!\!\left[\rho u \left(e + \frac{u^2}{2} + \frac{p}{\rho}\right)\right]\!\!\right] = 0, \tag{27}$$

$$[\![\rho u Y_i]\!] = 0, \qquad (i = 1, \ldots, N). \tag{28}$$

Substitution of Eq. (25) into Eq. (28) gives the standard result that species mass fractions are frozen through a discontinuity: $[\![Y_i]\!] = 0$. As a consequence, Eqs. (25-27) combined with Eqs. (5-6) form a set of five algebraic equations in the five unknowns ρ, u, p, e, and T which admit two physical solutions: the ambient state and the shock state.

The driving inhomogeneity of the system is the term $\dot{\omega}_i$ in Eq. (4). Examination of Eq. (9) reveals that r_j and thus $\dot{\omega}_i$ are driven to zero when

$$K_j^c(T) = \prod_{k=1}^{N} \left(\frac{\rho Y_k}{M_k}\right)^{(\nu''_{kj} - \nu'_{kj})}, \qquad (j = 1, \ldots, J). \tag{29}$$

A lengthy, but standard, analysis of Eq. (29) utilizing Eqs. (10, 22-23) reveals the equilibrium condition to be equivalent to

$$\sum_{i=1}^{N} \left(\nu''_{ij} - \nu'_{ij}\right) \mu_i = 0, \qquad (j = 1, \ldots, J), \tag{30}$$

which is easily shown to correspond to minimization of the Gibbs free energy.

B. Reduction of System

The assumptions and operations necessary to reduce the system to $N-L$ ODEs in $N-L$ unknowns are given next. For each atomic element $l = 1, \ldots, L$, multiply each side of Eq. (4) by the constant term $m_l \phi_{il}/M_i$, sum the result from $i = 1$ to N, and employ Eqs. (12) and (14) to obtain

$$\frac{\partial}{\partial t}(\rho y_l) + \frac{\partial}{\partial x}(\rho u y_l) = 0, \qquad (l = 1, \ldots, L). \tag{31}$$

This demonstrates that the mass of each atomic element is conserved. Moreover, when Eq. (31) is combined with Eq. (1), one finds that

$$\frac{\partial y_l}{\partial t} + u\frac{\partial y_l}{\partial x} = 0. \qquad (l = 1, \ldots, L). \tag{32}$$

That is, for a material fluid particle, there is no time rate of change of atomic element mass fraction. Consequently, atomic element mass fraction distributions in mixtures which are initially spatially homogeneous remain homogeneous. This study will only be concerned with such mixtures; consequently,

$$y_l(x,t) = y_{lo}, \qquad (l = 1, \ldots, L), \tag{33}$$

where the initial value of atomic element mass fractions y_{lo} can be fixed from initial conditions, which, from Eq. (24), are constrained so that $\sum_{l=1}^{L} y_{lo} = 1$. Here, the subscript "o" represents the undisturbed ambient state. Thus, one can apply this result to cast Eq. (14) as an underconstrained system of L linear equations in N unknowns ($L < N$):

$$y_{lo} \;=\; m_l \sum_{i=1}^{N} \frac{\phi_{il}}{M_i} Y_i, \qquad (l = 1, \ldots L). \tag{34}$$

Equation (34) can be rewritten into a variety of consistent row-echelon forms. Assuming the variables are ordered such that the last L entries for Y_i have non-zero pivots, one can invert Equation (34) to obtain

$$Y_{N-l+1} = \psi_l(Y_1, \ldots, Y_{N-L}; y_{1o}, \ldots, y_{Lo}, M_i, \phi_{i1}, \ldots, \phi_{iL}). \qquad (l = 1, \ldots, L). \tag{35}$$

Here ψ_l is a linear function of the first $N-L$ species mass fractions, parameterized by the atomic element mass fractions, molecular masses, and species atomic element indices. As a result, it is possible to replace the N equations given by Eqs. (4), $i = 1, \ldots, N-1$, and (7) by the N equations given by Eqs. (4), $i = 1, \ldots, N-L$, and (35), $l = 1, \ldots, L$.

It is now demanded that a stationary solution exists so that Eqs. (1-3) and the first $N - L$ of Eqs. (4) become the following ODEs in the spatial independent variable x,

$$\frac{d}{dx}(\rho u) = 0, \tag{36}$$

$$\frac{d}{dx}\left(\rho u^2 + p\right) = 0, \tag{37}$$

$$\frac{d}{dx}\left(\rho u\left(e + \frac{u^2}{2} + \frac{p}{\rho}\right)\right) = 0, \tag{38}$$

$$\frac{d}{dx}(\rho u Y_i) = \dot{\omega}_i M_i, \qquad (i = 1, \ldots, N-L). \tag{39}$$

Initial conditions are specified so that just before the shock jump at $x = 0^-$ one has

$$\rho(0^-) = \rho_o, \quad u(0^-) = D, \quad p(0^-) = p_o, \quad Y_i(0^-) = Y_{io}, \ (i = 1, \ldots, N-L). \tag{40}$$

Here, D represents the ambient fluid velocity. Then, using Eqs. (40) with Eqs. (5-6), one can find consistent values for

$$e(0^-) = e_o, \qquad T(0^-) = T_o. \tag{41}$$

The homogeneous Eqs. (36-38) can then be integrated to obtain extended Rankine-Hugoniot equations, and Eq. (39) can be simplified to obtain

$$\begin{aligned} \rho u &= \rho_o D, && (42)\\ \rho u^2 + p &= \rho_o D^2 + p_o, && (43)\\ e + \frac{u^2}{2} + \frac{p}{\rho} &= e_o + \frac{D^2}{2} + \frac{p_o}{\rho_o}, && (44)\\ \frac{dY_i}{dx} &= \frac{\dot{\omega}_i M_i}{\rho_o D}, \qquad (i = 1, \ldots, N-L). && (45) \end{aligned}$$

After defining the intermediate function $\sigma(Y_i)$ as

$$\sigma(Y_i) \equiv \sum_{i=1}^{N} \frac{Y_i}{M_i}, \tag{46}$$

a detailed algebraic analysis of Eqs. (5, 42-44) allows one to formulate an explicit expression for $\rho(T, Y_i)$:

$$\rho(T, Y_i) = \rho_o \frac{D^2}{\Re T \sigma(Y_i)} \left(1 + \frac{\Re T_o \sigma(Y_{io})}{D^2} \pm \sqrt{\left(1 + \frac{\Re T_o \sigma(Y_{io})}{D^2} \right)^2 - 4 \frac{\Re T \sigma(Y_i)}{D^2}} \right). \tag{47}$$

The "+" and "−" branches are associated with perturbations from the shock and inert states, respectively. Combining Eq. (47) with Eq. (42) gives $u(T, Y_i)$. Then, Eq. (43) can be used to obtain $p(T, Y_i)$, followed by use of Eq. (44) to get $e(T, Y_i)$. Combining the expression for $e(T, Y_i)$ with Eq. (6) as well as employing Eq. (35) yields an implicit algebraic relation between T and Y_i, $i = 1, \ldots, N-L$:

$$\begin{aligned} \sum_{i=1}^{N} Y_i \left(h_i^{ref} + \int_{T_{ref}}^{T} c_{pi}(\hat{T}) d\hat{T} - \frac{\Re T}{M_i} \right) - e_o + \frac{\Re T \sigma(Y_i)}{2} - \frac{\Re T_o \sigma(Y_{io})}{2} \left(1 - \frac{\Re T_o \sigma(Y_{io})}{2D^2} \right) \\ - \frac{D^2}{4} \left(1 \pm \left(1 + \frac{\Re T_o \sigma(Y_{io})}{D^2} \right) \sqrt{\left(1 + \frac{\Re T_o \sigma(Y_{io})}{D^2} \right)^2 - 4 \frac{\Re T \sigma(Y_i)}{D^2}} \right) = 0. \end{aligned} \tag{48}$$

One can use Newton iteration on Eq. (48) to determine $T(Y_i)$. Thus for given Y_i's, one gets T, and then ρ, u, p, and e.

This study will deal exclusively with the shock ("+") branch, and will consider the fixed shock to be located at $x = 0$. A fluid particle approaching from $x < 0$ encounters the shock, decelerates, and proceeds at a slower speed in the direction of increasing x. If one were to apply a Galilean transformation to this system with frame velocity D, it is clear that this also describes a wave traveling at speed D in the direction of decreasing x into a fluid at rest. So one can interpret D as the classical detonation wave speed. Also, it is easily shown that below a critical value of D, no real solution exists. This is an extension of the classical CJ condition.

Endowed with effective representations of dependent variables in terms of the $N-L$ species mass fractions, one can then use Eq. (8) to obtain $\dot{\omega}_i(Y_1, \ldots, Y_{N-L})$. In the same way, one obtains all auxiliary variables in Eqs. (14-24) as functions of $Y_1, \ldots, Y_{N-L}$. Consequently, it is possible to write Eq. (45) and the relevant part of Eq. (40) as a set of non-linear ODEs and initial conditions in the standard form

$$\frac{dY_i}{dx} = f_i(Y_1, \ldots, Y_{N-L}), \qquad Y_i(0^-) = Y_{io}, \qquad (i = 1, \ldots, N-L), \tag{49}$$

where f_i is a non-linear function of the dependent variables given by $f_i = \dot{\omega}_i M_i / (\rho_o D)$. While in certain special cases, *e.g.* reactions which each preserve the number of molecules so that more conserved variables exist, in general, Eqs. (49) are the minimal set necessary to describe the steady spatial structure of a gas phase detonation in a system which is described by detailed kinetics.

C. Length Scale Analysis

One can apply a standard eigenvalue analysis to Eqs. (49) to accurately estimate the local length scales over which the system evolves. Defining, for convenience, the column vector $\mathbf{y} = Y_i$, $i = 1, \ldots, N - L$, consider a point $x = x^*$ at which $\mathbf{y} = \mathbf{y}^*$, which may or may not be near an equilibrium state. Assuming that the local Jacobian matrix of f_i, taken to be $\mathbf{J} = \partial f_i / \partial Y_j \big|_{\mathbf{y}^*}$, is non-singular, one can linearize Eq. (49) to arrive at

$$\frac{d\mathbf{y}}{dx} = \mathbf{J} \cdot (\mathbf{y} - \mathbf{y}^*) + \mathbf{b}, \qquad \mathbf{y}(x^*) = \mathbf{y}^*. \tag{50}$$

Here, $\mathbf{b}$ is a constant column vector of dimension $N - L$, and $\mathbf{J}$ has dimension $(N - L) \times (N - L)$. When $\mathbf{b} = \mathbf{0}$, the state $\mathbf{y} = \mathbf{y}^*$ corresponds to an equilibrium state. As described by Fickett and Davis[1], one can expect singular behavior near sonic points. Extreme care must be exercised in such circumstances; it is often the case that detailed kinetics can induce the true propagation speed of an unsupported detonation to deviate from that given by a classical CJ analysis. To avoid such concerns, this study only considers waves which are traveling slightly faster than the CJ speed, which physically suggests the presence of weak piston support.

Next, define a new dependent variable $\mathbf{z}$ such that

$$\mathbf{z} = \mathbf{y} - \mathbf{y}^* + \mathbf{J}^{-1} \cdot \mathbf{b}. \tag{51}$$

Eliminating $\mathbf{y}$ from Eq. (50) in favor of $\mathbf{z}$, one gets

$$\frac{d\mathbf{z}}{dx} = \mathbf{J} \cdot \mathbf{z}, \qquad \mathbf{z}(x^*) = \mathbf{J}^{-1} \cdot \mathbf{b}. \tag{52}$$

Assuming that $\mathbf{J}$ has a complete set of $N - L$ linearly independent eigenvectors, one can decompose $\mathbf{J}$ as $\mathbf{J} = \mathbf{P} \cdot \mathbf{\Lambda} \cdot \mathbf{P}^{-1}$, where $\mathbf{P}$ is the matrix whose columns are populated by the right eigenvectors of $\mathbf{J}$, and $\mathbf{\Lambda}$ is the diagonal matrix whose diagonal is composed of the eigenvalues, $\lambda_i, i = 1, \ldots, N - L$, of $\mathbf{J}$. If an insufficient number of linearly independent eigenvectors are available, a Jordan decomposition can be used to obtain an equivalent result. Thus, Eq. (52) can be written as

$$\frac{d\mathbf{z}}{dx} = \mathbf{P} \cdot \mathbf{\Lambda} \cdot \mathbf{P}^{-1} \cdot \mathbf{z}, \qquad \mathbf{z}(x^*) = \mathbf{J}^{-1} \cdot \mathbf{b}. \tag{53}$$

Applying the locally constant matrix operator $\mathbf{P}^{-1}$ to both sides and defining $\mathbf{w} = \mathbf{P}^{-1} \cdot \mathbf{z}$, Eq. (53) transforms to the uncoupled set of equations

$$\frac{d\mathbf{w}}{dx} = \mathbf{\Lambda} \cdot \mathbf{w}, \qquad \mathbf{w}(x^*) = \mathbf{P}^{-1} \cdot \mathbf{J}^{-1} \cdot \mathbf{b}. \tag{54}$$

Their solutions are

$$\mathbf{w}(x) = e^{\mathbf{\Lambda}(x - x^*)} \cdot \mathbf{P}^{-1} \cdot \mathbf{J}^{-1} \cdot \mathbf{b}. \tag{55}$$

The convenient matrix exponential notation has been utilized, which is described in many standard texts, *cf.* Strang[20]. Obviously, the i^{th} component of $\mathbf{w}$ evolves on a local length scale ℓ_i given by

$$\ell_i = \frac{1}{|\mathrm{Re}\,(\lambda_i)\,|}, \qquad (i = 1, \ldots, N - L). \tag{56}$$

This is the key result which will give the local length scales at all points in the reaction zone up to and including the equilibrium point. In the bulk of the detonation reaction zone structure, the eigenvalues are purely real. For the limited regions in which they are complex, the real part gives the length scale of amplitude growth, and the imaginary part gives an additional length scale of oscillation.

It is generally impossible to associate the evolution of a particular species with a particular eigenvalue since the species mass fractions depend on local linear combinations of all components of $\mathbf{w}$ and thus include evolution on *all* of the $N - L$ length scales of the system. This is seen by reconstructing $\mathbf{y}$, from which one finds that the local evolution of the species mass fractions is described by

$$\mathbf{y}(x) = \mathbf{y}^* + \left(\mathbf{P} \cdot e^{\mathbf{\Lambda}(x - x^*)} \cdot \mathbf{P}^{-1} - \mathbf{I} \right) \cdot \mathbf{J}^{-1} \cdot \mathbf{b}. \tag{57}$$

Since this analysis is local, the eigenvalues, and thus the length scales, will vary with x; that is, one has $\lambda_i(x)$ and $\ell_i(x)$ throughout the reaction zone.

The analysis of this section gives the framework for a local description of the evolution of a finite set of chemical length scales, fixed by kinetic rates and satisfaction of conservation properties. As an aside, one can ask how the presence of additional mechanisms such as diffusion and unsteadiness would influence the local length scales. In the one-dimensional steady limit, each additional diffusion mechanism, *e.g.*, species, momentum, energy, adds a single ODE to the set, and thus a new length scale. This could easily be analyzed in the manner already presented.

The addition of unsteadiness is more complicated, as such a system is described by a set of partial differential equations (PDEs). In terms of the analysis of this section, one may consider the system of PDEs to be, after spatial discretization, a very large set of ODEs in time. A related eigenvalue analysis could be performed on the system's Jacobian, and a set of local time scales of evolution is available at each point in time. These time scales would exhibit, in general, full coupling between reaction, convection, and diffusion. In fact, one can show in the limit as the spatial discretization approaches zero, that most time scales become increasingly dominated by diffusion, and the minimum time scale is on the order of the square of the spatial discretization size. In order for the error in an unsteady calculation which includes diffusion to be converging to zero, one must have a discretization fine enough to render the diffusive time scales finer than the chemical time scales. This poses a serious computational challenge for most physically important problems.

III. Computational Method

All calculations were performed on a single processor Sun Blade 1000 with a speed of 900 MHz. Typical calculations done in double precision were completed within two minutes. A Fortran 90 code that drew upon standard IMSL routines DNEQNF for Newton iteration, DFDJAC for Jacobian evaluation, and DEVLRG for eigenvalue computation was used. For evaluation of thermochemical properties, subroutines available in a double precision version of the public domain edition of the Chemkin[21] package were utilized; no other general Chemkin tools for solving specific physical problems were employed. This package draws upon a standard thermodynamic data base which contains properties for a wide variety of constituents; these include coefficients for polynomial curve fits for the variation of specific heats with temperature.

For integration, three methods were used: 1) a first order explicit Euler method, 2) a second order explicit Runge-Kutta method, and 3) an implicit Adams method with functional iteration as embodied in the standard code DLSODE[22] in which step sizes were adapted to achieve a user-defined absolute error tolerance, here taken as 10^{-14}. When all methods were run with a spatial discretization smaller than the smallest physical length scale, the predictions were virtually indistinguishable. The explicit Euler and Runge-Kutta codes utilized a constant spatial discretization step size which was useful in grid convergence and numerical stability studies. The implicit Adams method was used in studies to obtain the complete reaction zone structure; here it was straightforward to adjust the spatial discretization step so as to generate detailed results in the induction zone, and coarser results near equilibrium. However, even near equilibrium, it was seen that the number of internal steps taken to achieve the error tolerance was consistent with the discretization at the spatial scale dictated by the finest physical scale.

IV. Results

Results are presented for hydrogen-air mixtures which are initially in a stoichiometric molar ratio of $2H_2 + O_2 + 3.76N_2$. A kinetic model with $N = 9$ species, $L = 3$ atomic elements, and $J = 19$ reversible reactions, identical to that employed by Shepherd[3] in his hydrogen-air calculations, is used, and is reported in detail in Table 1. Obviously there are many slightly different kinetic models from which to choose, and the differences in each may become apparent in sensitive regions of the reaction zone structure. However, analyzing the differences among the various kinetic models is beyond the scope of this study. The nine species modeled are H, O, H_2, O_2, OH, H_2O, HO_2, H_2O_2, and N_2. Nitrogen is regarded as an inert diluent. The three atomic elements are H, O, and N. Shepherd extracts this model from the more general model reported by Miller, *et al.*[23] The kinetic model is nearly identical to that reported by Mikolaitis[4], who has an obvious transcription error in his value for A_4. As use of this reported value has catastrophic consequences for the calculation, and Mikolaitis' results agree with Shepherd's and those of this study, it is likely that the correct value for A_4 was actually used in Ref. 4.

A. Stoichiometric CJ Hydrogen-Air Detonation at Standard Conditions

The model was used on a mixture, which in its unshocked state was at $p_o = 1\ atm$ and $T_o = 298\ K$, under near-CJ conditions, defined by the state in which the Mach number at the equilibrium state approaches unity. The CJ state was determined by iteration and was found to be extremely sensitive to the initial velocity D. As the resulting length scales were relatively insensitive to D, a final state with a Mach number slightly less than unity was tolerated. A table of values of various thermochemical and dynamic properties at the initial state, shock state, and equilibrium state is given in Table 2. Here, in order to allow comparison with Refs. 3 and 4, mole fractions, in addition to mass fractions are reported. All figures, with the exception of one in which p_o is varied, are for simulations performed at the conditions of Table 2.

Figure 1 gives a plot of the spatial distribution of species mole fractions throughout the reaction zone. This calculation was performed with the Adams implicit method embodied in DLSODE. Results can be directly compared to those of Shepherd, who reports predictions over the reaction zone length scale whose structures can be discerned down to the induction zone length scale, but not at the finest scales. The use of log-log scaling in Fig. 1 reveals a variety of scales over which the mole fractions evolve. The shock front is located at $x = 0\ cm$. Just past the shock, collisions of the major species H_2, O_2, and N_2 commence with more vigor, and minor species are generated. For very small distances from the shock front $0 < x < 10^{-4}\ cm$, the mole fractions of minor species H, O, OH, H_2O, HO_2, and H_2O_2 grow at rates which are well modeled by power laws, while major species mole fractions are essentially unchanged. At $x \sim 10^{-4}\ cm$, one notices the slopes of some of the curves, *e.g.* that for OH, begin to change; this indicates that, at this scale, there is beginning to be significant chemical interactions of the minor species. For $10^{-4} < x < 10^{-2}\ cm$, major species collisions continue, minor species mole fractions continue to rapidly grow, and the minor species continue to interact. Just past $x = 10^{-2}\ cm$, a particularly vigorous stage of the reaction ensues in which all species mole fractions, except the inert N_2, undergo significant change. This region is considered to be near the end of the induction zone, whose boundary is typically defined by the point at which the temperature gradient dT/dx reaches a maximum value. With this definition, the induction zone thickness is found to be $2.6 \times 10^{-2}\ cm$. It is also the beginning of the thermal explosion zone, which extends from roughly $2.6 \times 10^{-2} < x < 3 \times 10^{-2}\ cm$. This is followed by a relatively long recombination zone, $3 \times 10^{-2} < x < 10^{0}\ cm$, in which radicals recombine exothermically into the predominant product species, H_2O. For $x > 10^{0}\ cm$, it is clear from Fig. 1 that the system has come to an equilibrium, as all spatial gradients are near zero. This is confirmed by calculating the equilibrium state with an iterative Newton solver for $f_i(Y_i, \ldots, Y_{N-L}) = 0$.

Plots of temperature and pressure in the reaction zone are given in Figs. 2 and 3, respectively. In these figures the induction zone is clearly shown as a region of essentially constant temperature and pressure. This seeming tranquility masks the real underlying evolution of species mole fractions which is occurring within this zone. In contrast, the variation of pressure and temperature in the recombination zone is mild in comparison.

The multi-scale nature of the problem is most clearly displayed in Fig. 4. Here the length scales $\ell_i(x)$ predicted by the local eigenvalue analysis described earlier are shown as functions of the distance from the shock. Each curve corresponds to the reciprocal of the absolute value of the real part of an eigenvalue. Most importantly, the finest length scale is seen to vary from near $10^{-4}\ cm$ in the induction zone to as low as $2.3 \times 10^{-5}\ cm$ in the recombination zone. Such scales are likely close to mean free path length scales, and thus this continuum calculation is probably approaching its lower limit of validity. In fact, a simple independent Navier-Stokes calculation of an comparable inert viscous shock structure reveals that the viscous length scales are precisely the same order of magnitude as the finest reaction length scales. This is likely a consequence of both constitutive models for reaction and diffusion having molecular collisions as causal forces.

It is noted here that the present analysis serves to correct a speculation made in Ref. 12, where it was inferred, from a time scale analysis that did not include a detailed consideration of species convection, that length scales would be predicted which would give rise to a violation of the continuum assumption.

The largest length scales range from around $3 \times 10^{1}\ cm$ in the induction zone to around $3 \times 10^{-1}\ cm$ at equilibrium state. The smallest length scale is consistent with the scale on which mole fractions are seen to vary in Fig. 1. Moreover, the smallest scale is roughly equal to the internal step size utilized by the adaptive DLSODE integration subroutine, in which the size of the integration step is automatically chosen to maintain stability as well as achieve the specified accuracy. The largest length scale is not as critical, but does provide a useful estimate of the overall length of the reaction zone.

Additional features of Fig. 4 are noteworthy. For the bulk of the domain, there are $N - L = 6$ real

and distinct eigenvalues. For $x < 3 \times 10^{-2}$ cm, five of these eigenvalues have negative real parts, and one has a positive real part, indicating growth of a local eigenmode. For $x > 3 \times 10^{-2}$ cm, the real parts of all six eigenvalues are negative, indicating a relaxation to equilibrium. The spike in one of the curves near $x = 3 \times 10^{-2}$ cm indicates one of the eigenvalues has a real part passing through zero; hence, its reciprocal approaches infinity. In a few isolated regions near the end of the induction zone and in the thermal explosion zone, some of the eigenvalues are complex conjugates. This is indicative of a local oscillatory behavior and is seen in Fig. 4 when some of the curves merge in a thin zone. While a few curves appear to cross, a fine scale calculation shows that they in fact remain distinct, even when up to three orders of magnitude increase in resolution is employed.

B. Effect of Initial Pressure

A series of calculations in the same mixture held at the same temperature was performed in which the initial pressure varied from 0.5 to 3.0 atm. Again, detonations which were very near to the CJ state were studied, and both the finest length scale given by the eigenvalue analysis as well as the induction length scale were predicted. Results are summarized in Fig. 5. Here it is clearly demonstrated that the smallest length scale is roughly three orders of magnitude finer than that of the induction zone. The predictions of the induction zone length compare well with those given in Ref. 5, where the same physical problem was modeled with a slightly different kinetics model.

C. Verification

Two types of verification of the predictions are given here: 1) a comparison to Mikolaitis'[4] detailed induction zone predictions, and 2) a formal grid convergence study. For the first verification, some small adjustments are necessary. In Ref. 4 only the induction zone was considered, and p, T, and u were frozen at their post-shock values. Then the governing equations were integrated numerically in time, and results compared favorably to those of a detailed asymptotic theory. In order to properly compare predictions, the time coordinate of a Lagrangian particle must be obtained by numerical integration of the equation for particle velocity, $u = dx/dt$. As $u(x)$ is available after solution of Eq. (49), the local time can be found by the quadrature

$$t = \int_0^x \frac{d\hat{x}}{u(\hat{x})}. \tag{58}$$

Using this result, it is then possible to plot the variation of all thermochemical properties of a fluid particle as a function of the relative time after which it has passed the shock located at $x = 0$. Such a plot is given in Fig. 6 for the mole fractions of all species in the induction zone. The features are roughly the same as those seen in Fig. 1. A direct comparison to the predictions of Ref. 4 shows excellent agreement for all variables.

For the second verification, a formal grid convergence study is performed over a wide range of spatial discretization levels: $5 \times 10^{-11} < \Delta x < 10^{-4}$ cm. While the finest discretization scales are definitely below the continuum limit, for purposes of mathematical verification of the numerical method, this is inconsequential. Conditions were identical to those used to predict Fig. 1. As it was desirable to use a fixed value of Δx in an individual calculation, use of the adaptive DLSODE was discarded in favor of a simpler first order explicit Euler and second order explicit Runge-Kutta method. While both of these methods work well over the entire reaction zone, it was more efficient to determine the convergence properties by integrating only to a small final value of distance, here taken to be $x = 10^{-4}$ cm. As this final value of x is as small as the finest length scale, it is guaranteed there will be no problems with numerical stability.

Figure 7 shows the results of the grid convergence study. First, results were obtained on a highly refined grid with $\Delta x = 10^{-11}$ cm for the second order method. These were taken as a benchmark solution to which comparisons could be made. Next, it was chosen to compare the mole fraction values of a minor species, X_{OH}, at the final point $x = 10^{-4}$ cm to the prediction of the benchmark case. For each discretization and integration method, a value of the relative error, ε_{OH},

$$\varepsilon_{OH} = \left| \frac{X_{OH,approximate} - X_{OH,benchmark}}{X_{OH,benchmark}} \right|_{x=10^{-4}\ cm},$$

was calculated. Had other variables been chosen or an error norm encompassing a broader domain been chosen, the convergence rates would not have been affected.

The first order Euler method in fact gives error predictions which converge at a rate of 1.006, effectively equivalent to its expected value. At the smallest $\Delta x = 5 \times 10^{-11}$ cm studied, the method is still converging, and has not yet reached its machine roundoff limit. The second order Runge-Kutta method predicts errors to converge at a rate of 2.008, again equivalent to its expected value. Its error is always lower than that of the first order method, and near $\Delta x = 2 \times 10^{-9}$ cm, it appears that the machine roundoff limit has been reached as further refinement results in no improvement in the error. The actual relative error at this limit is just under 10^{-10} which indicates that the accuracy exceeds that of single precision. It is likely that the strict double precision limit of 10^{-16} is not reached because of the effects of accumulation of roundoff error after many millions of operations.

D. Numerical Stability

A series of calculations was subsequently performed at discretization levels near the threshold of numerical instability. Conditions again were identical to those used to predict Fig. 1. Figure 8 shows predictions of X_H over the range $0 < x < 5 \times 10^{-3}$ cm using a first order explicit Euler integration. Similar results could have been obtained for other variables or using other integration schemes; it is difficult, however, for the subroutine DLSODE to generate spatially unstable numerical results as it uses automatic step size selection to prevent this from happening. Thus, in effect DLSODE is providing an atypical adaptive mesh refinement (AMR). In more challenging spatio-temporal problems, multi-scale effects often require adaptation in space *and* time. In such cases, solvers like DLSODE are confined to adaptation in time; independent algorithms, such as the Wavelet Adaptive Multilevel Representation (WAMR), see Ref. 12, are required to address the multi-scaled spatial structures. This extension to adaptation in space and time is non-trivial.

For a value of $\Delta x = 1.00 \times 10^{-5}$ cm, well below the finest physical length scale predicted by the eigenvalue analysis, the evolution of X_H is well-behaved. Increasing Δx to a value in the neighborhood of the smallest physical length scale, $\Delta x = 2.00 \times 10^{-4}$ cm results in a prediction which is oscillatory but stable. Increasing the discretization length slightly to $\Delta x = 2.38 \times 10^{-4}$ cm triggers an unstable numerical oscillation.

If one were to model a similar detonation using a computational model which allowed for both time and space variation and one were to choose a computational grid which did not capture the finest physical length scale, the following result would be likely. In the steady state limit, the model would be inclined to predict relaxation to a spatially oscillatory state similar to that shown in the large Δx case of Fig. 8. Such oscillations are damped, however, in the unsteady model by artificial diffusion which depends on both the grid and computational algorithm employed. This may account for the wide disparity in the small scale structures that one often sees in predictions of identical cases by either the same algorithm on different grids, different algorithms on the same grid, or even the same algorithm and same grid on different computers.

E. Comparison with Recent Results

Finally, predictions of the current algorithm are compared with some of the best calculations of detonations in hydrogen-based systems which have appeared in the recent archival literature. The results are summarized in Table 3, which most importantly, lists the induction zone length, ℓ_{ind}, the finest length predicted by the eigenvalue analysis, ℓ_f, and the grid discretization, Δx, employed in the study. For each case, the algorithm presented here was exercised on the published models under the appropriate conditions reported. The induction length scale obtained for the low pressure $H_2 + 2O_2 + 7Ar$ case agrees with the result reported in Ref. 8 but not with that reported in Ref. 6. It is believed that the value reported in Ref. 6 (2×10^{-3} cm) is a typographical error since agreement is obtained with other reported values from Ref. 6. The key result found in Table 3 is that none of these independent studies has captured ℓ_f, and some do not capture ℓ_{ind}. While these are some of the best calculations, it is not difficult to find worse cases in the literature.

V. Conclusions

It has been unambiguously shown that the finest length scales predicted by a one-dimensional steady analysis of a common stoichiometric CJ hydrogen-air detonation model under standard atmospheric conditions are roughly three orders of magnitude finer than the induction zone thickness. Consequently, many modern calculations using detailed kinetics coupled with a strategy to resolve at most the induction zone are formally under-resolved. It is also clear that in order to meet the strictest demands of rigorous scientific computing for detonations with detailed kinetics, one must employ a computational grid with a characteristic

length at or below the values predicted by the present analysis. In fact when other physics is considered, such as detonations with curvature[24], or those in which high wavenumber instabilities are present[25], the demands of spatial resolution may be even more stringent than those suggested here. Furthermore, as preliminary calculations indicate the finest reaction zone length scales are of the same order as diffusion length scales in shocks, it may be the case that a resolved model of detonation which includes detailed kinetics may need to consider diffusion.

That under-resolved computations often produce plausible results is understandable when one considers that a wide variety of calculations are driving towards a stable equilibrium state which is fixed by path-independent thermodynamics. It is often the case that these near-equilibrium properties are the easiest to predict as well as observe. However, for many classes of problems, such as those with inherent unsteadiness, the journey is as important as the destination, and agreement with equilibrium wave speeds, pressures, and temperatures, is a necessary but insufficient requirement. In such cases, the journey is only properly completed when the spatial structures are properly resolved. Short cuts to equilibrium provided by under-resolved paths do not reflect the full richness of the process and run the risk of leading the journey to a non-physical catastrophe.

It is often argued that such fine discretizations are not necessary as the small scales will not influence the scales of engineering importance. First, such a conclusion cannot be made *a priori*; indeed, the field of non-linear dynamics provides many counter-examples in which small scale disturbances ultimately manifest themselves on a large scale. Lorenz's[26] now-celebrated study of transition to chaos is but one such case. So, until such calculations are actually made which prove the unimportance of small scales, the possibility of their relevance cannot be cavalierly dismissed. Second, if it is indeed the case that these small scales are of no consequence, then it is appropriate for the modeling community to employ only mathematical models which do not contain such inherently fine scales. To argue on one hand that it is critical that modern engineering applications require a consideration of detailed chemical kinetics and on the other hand that fine scale phenomena are of no consequence is scientifically incoherent. That said, the present study is incapable of answering the critical question of how important the fine scale structures are. It just provides a simple diagnosis that most computational combustion results in the literature are afflicted with under-resolution. The prognosis, however, can still be bright, but only if a careful regimen of detailed, resolved calculations of key physical problems, transparently presented so that a skeptical broader community can have full confidence in the predictions, is undertaken.

References

[1] Fickett, W., and Davis, W. C., *Detonation*, University of California Press, Berkeley, 1979.

[2] Westbrook, C. K., "Hydrogen Oxidation Kinetics in Gaseous Detonations," *Combustion Science and Technology*, Vol. 29, Nos. 1-2, 1982, pp. 67-81.

[3] Shepherd, J. E., "Chemical Kinetics of Hydrogen-Air-Diluent Detonations," *Dynamics of Explosions*, edited by J. R. Bowen, J.-C. Leyer, and R. I. Soloukhin, Vol. 106, Progress in Astronautics and Aeronautics, AIAA, New York, 1986, pp. 263-293.

[4] Mikolaitis, D. W., "An Asymptotic Analysis of the Induction Phases of Hydrogen-Air Detonations," *Combustion Science and Technology*, Vol. 52, Nos. 4-6, 1987, pp. 293-323.

[5] Lu, T., Law, C. K., and Ju, Y., "Some Aspects of Chemical Kinetics in Chapman-Jouguet Detonation: Induction Length Analysis," *Journal of Propulsion and Power*, Vol. 19, No. 5, 2003, pp. 901-907.

[6] Oran, E. S., Weber, J. W., Stefaniw, E. I., Lefebvre, M. H., and Anderson, J. D., "A Numerical Study of a Two-Dimensional $H_2 - O_2 - Ar$ Detonation Using a Detailed Chemical Reaction Model," *Combustion and Flame*, Vol. 113, Nos. 1-2, 1998, pp. 147-163.

[7] Eckett, C. A., Quirk, J. J., and Shepherd, J. E., "The Role of Unsteadiness in Direct Initiation of Gaseous Detonations," *Journal of Fluid Mechanics*, Vol. 421, 2000, pp. 147-183.

[8] Pintgen, F., Eckett, C. A., Austin, J. M., and Shepherd, J. E., "Direct Observations of Reaction Zone Structure in Propagating Detonations," *Combustion and Flame*, Vol. 133, No. 3, 2003, pp. 211-229.

[9] Sheffer, S. G., Martinelli, L., and Jameson, A., "An Efficient Multigrid Algorithm for Compressible Reactive Flows," *Journal of Computational Physics*, Vol. 144, No. 2, 1998, pp. 484-516.

[10] Sheffer, S. G., Martinelli, L., and Jameson, A., "Simulation of Reacting Hydrocarbon Flows with Detailed Chemistry," *Combustion Science and Technology*, Vol. 136, Nos. 1-6, 1998, pp. 55-80.

[11] Tsuboi, N., Katoh, S., and Hayashi, A. K., "Three-Dimensional Numerical Simulation for Hydrogen/Air Detonation: Rectangular and Diagonal Structures," *Proceedings of the Combustion Institute*, Vol. 29, 2002, pp. 2783-2788.

[12] Singh, S., Rastigejev, Y., Paolucci, S., and Powers, J. M., "Viscous Detonation in $H_2 - O_2 - Ar$ Using Intrinsic Low-Dimensional Manifolds and Wavelet Adaptive Multilevel Representation," *Combustion Theory and Modelling*, Vol. 5, No. 2, 2001, pp. 163-184.

[13] Fedkiw, R. P., Merriman, B., and Osher, S., "High Accuracy Numerical Methods for Thermally Perfect Gas Flows with Chemistry," *Journal of Computational Physics*, Vol. 132, No. 2, 1997, pp. 175-190.

[14] Ebrahimi, H. B., and Merkle, C. L., "Numerical Simulation of a Pulse Detonation Engine with Hydrogen Fuels," *Journal of Propulsion and Power*, Vol. 18, No. 5, 2002, pp. 1042-1048.

[15] Dudebout, R., Sislian, J. P., and Oppitz, R., "Numerical Simulation of Hypersonic Shock-Induced Combustion Ramjets," *Journal of Propulsion and Power*, Vol. 14, No. 6, 1998, pp. 869-879.

[16] He, X., and Karagozian, A. R., "Numerical Simulation of Pulse Detonation Engine Phenomena," *Journal of Scientific Computing*, Vol. 19, Nos. 1-3, 2003, pp. 201-224.

[17] Sichel, M., Tonello, N. A., Oran, E. S., and Jones, D. A., "A Two-Step Kinetics Model for Numerical Simulation of Explosions and Detonations in $H_2 - O_2$ Mixtures," *Proceedings of the Royal Society of London*, Series A, Vol. 458, 2002, pp. 49-82.

[18] Kawai, S., and Fujiwara, T., "Numerical Analysis of First and Second Cycles of Oxyhydrogen Pulse Detonation Engine," *AIAA Journal*, Vol. 41, No. 10, 2003, pp. 2013-2019.

[19] Korobeinikov, V. P., Levin, V. A., Markov, V. V., and Chernyi, G. G., "Propagation of Blast Waves in a Combustible Gas," *Astonautica Acta*, Vol. 17, 1972, pp. 529-537.

[20] Strang, G., *Linear Algebra and its Applications*, Third Edition, Harcourt Brace Jovanovich, Fort Worth, Texas, 1988.

[21] Kee, R. J., Rupley, F. M., and Miller, J. A., "The Chemkin Thermodynamic Data Base," Sandia National Laboratories Report, SAND87-8215B, 1990.

[22] Hindmarsh, A. C., "ODEPACK, a Systematized Collection of ODE Solvers," *Scientific Computing*, edited by R. S. Stepleman, *et al.*, North Holland, Amsterdam, 1983, pp. 55-64.

[23] Miller, J. A., Mitchell, R. E., Smooke, M. D., and Kee, R. J., "Toward a Comprehensive Chemical Kinetic Mechanism for the Oxidation of Acetylene: Comparison of Model Predictions with Results from Flame and Shock Tube Experiments," *Proceedings of the Combustion Institute*, Vol. 19, 1982, pp. 181-196.

[24] He, L., "Theoretical Determination of the Critical Conditions for the Direct Initiation of Detonations in Hydrogen-Oxygen Mixtures,"' *Combustion and Flame*, Vol. 104, No. 4, 1996, pp. 401-418.

[25] Short, M., and Sharpe, G. J., "Pulsating Instability of Detonations with a Two-Step Chain-Branching Reaction Model: Theory and Numerics," *Combustion Theory and Modelling*, Vol. 7, No. 2, 2003, pp. 401-416.

[26] Lorenz, E. N., "Deterministic Nonperiodic Flow," *Journal of the Atmospheric Sciences*, Vol. 20, 1963, pp. 130-141.

j	Reaction	A_j	β_j	E_j
1	$H_2 + O_2 \rightleftharpoons OH + OH$	1.70×10^{13}	0.00	47780
2	$OH + H_2 \rightleftharpoons H_2O + H$	1.17×10^{9}	1.30	3626
3	$H + O_2 \rightleftharpoons OH + O$	5.13×10^{16}	−0.82	16507
4	$O + H_2 \rightleftharpoons OH + H$	1.80×10^{10}	1.00	8826
5	$H + O_2 + M \rightleftharpoons HO_2 + M$	2.10×10^{18}	−1.00	0
6	$H + O_2 + O_2 \rightleftharpoons HO_2 + O_2$	6.70×10^{19}	−1.42	0
7	$H + O_2 + N_2 \rightleftharpoons HO_2 + N_2$	6.70×10^{19}	−1.42	0
8	$OH + HO_2 \rightleftharpoons H_2O + O_2$	5.00×10^{13}	0.00	1000
9	$H + HO_2 \rightleftharpoons OH + OH$	2.50×10^{14}	0.00	1900
10	$O + HO_2 \rightleftharpoons O_2 + OH$	4.80×10^{13}	0.00	1000
11	$OH + OH \rightleftharpoons O + H_2O$	6.00×10^{8}	1.30	0
12	$H_2 + M \rightleftharpoons H + H + M$	2.23×10^{12}	0.50	92600
13	$O_2 + M \rightleftharpoons O + O + M$	1.85×10^{11}	0.50	95560
14	$H + OH + M \rightleftharpoons H_2O + M$	7.50×10^{23}	−2.60	0
15	$H + HO_2 \rightleftharpoons H_2 + O_2$	2.50×10^{13}	0.00	700
16	$HO_2 + HO_2 \rightleftharpoons H_2O_2 + O_2$	2.00×10^{12}	0.00	0
17	$H_2O_2 + M \rightleftharpoons OH + OH + M$	1.30×10^{17}	0.00	45500
18	$H_2O_2 + H \rightleftharpoons HO_2 + H_2$	1.60×10^{12}	0.00	3800
19	$H_2O_2 + OH \rightleftharpoons H_2O + HO_2$	1.00×10^{13}	0.00	1800

Table 1. Nine species, nineteen step reversible reaction mechanism for a hydrogen/oxygen/nitrogen mixture extracted from Ref. 23 and used in Refs. 3 and 4. The value of A_4 from Ref. 4 has been corrected to be consistent with earlier references. Units of A_j are in appropriate combinations of cm, mol, s, and K so that $\dot{\omega}_i$ has units of $mol/cm^3/s$; units of E_j are cal/mol. Third body collision efficiencies with M are $k_5(H_2O) = 21$, $k_5(H_2) = 3.3$, $k_{12}(H_2O) = 6$, $k_{12}(H) = 2$, $k_{12}(H_2) = 3$, $k_{14}(H_2O) = 20$.

Property	Units	Initial	Shock	CJ
p	atm	1.0000×10^{0}	2.7954×10^{1}	1.6269×10^{1}
T	K	2.9800×10^{2}	1.5427×10^{3}	2.9821×10^{3}
u	cm/s	1.9797×10^{5}	3.6661×10^{5}	1.0660×10^{5}
ρ	g/cm^3	8.5523×10^{-4}	4.6181×10^{-3}	1.5882×10^{-3}
γ		1.4009×10^{0}	1.3178×10^{0}	1.2440×10^{0}
M		4.8594×10^{0}	4.0779×10^{-1}	9.3824×10^{-1}
Y_{O_2}		2.2626×10^{-1}	2.2626×10^{-1}	1.3755×10^{-2}
Y_H		0.0000×10^{-0}	0.0000×10^{-0}	2.7105×10^{-4}
Y_{OH}		0.0000×10^{-0}	0.0000×10^{-0}	1.4820×10^{-2}
Y_O		0.0000×10^{-0}	0.0000×10^{-0}	1.7806×10^{-3}
Y_{H_2}		2.8522×10^{-2}	2.8522×10^{-2}	2.5670×10^{-3}
Y_{H_2O}		0.0000×10^{-0}	0.0000×10^{-0}	2.2166×10^{-1}
Y_{HO_2}		0.0000×10^{-0}	0.0000×10^{-0}	2.2350×10^{-5}
$Y_{H_2O_2}$		0.0000×10^{-0}	0.0000×10^{-0}	3.0765×10^{-6}
Y_{N_2}		7.4512×10^{-1}	7.4512×10^{-1}	7.4512×10^{-1}
X_{O_2}		1.4793×10^{-1}	1.4793×10^{-1}	1.0269×10^{-2}
X_H		0.0000×10^{-0}	0.0000×10^{-0}	6.4242×10^{-3}
X_{OH}		0.0000×10^{-0}	0.0000×10^{-0}	2.0818×10^{-2}
X_O		0.0000×10^{-0}	0.0000×10^{-0}	2.6588×10^{-3}
X_{H_2}		2.9586×10^{-2}	2.9586×10^{-2}	3.0421×10^{-2}
X_{H_2O}		0.0000×10^{-0}	0.0000×10^{-0}	2.9395×10^{-1}
X_{HO_2}		0.0000×10^{-0}	0.0000×10^{-0}	1.6177×10^{-5}
$X_{H_2O_2}$		0.0000×10^{-0}	0.0000×10^{-0}	2.1607×10^{-6}
X_{N_2}		5.5621×10^{-1}	5.5621×10^{-1}	6.3544×10^{-1}

Table 2. Thermochemical and dynamic properties for a mixture of $2H_2 + O_2 + 3.76N_2$.

Ref.	Mixture	T_o (K)	p_o (atm)	ℓ_{ind} (cm)	ℓ_f (cm)	Δx (cm)
6	$2H_2 + O_2 + 7Ar$	2.98×10^{2}	6.58×10^{-2}	1.47×10^{-1}	2.17×10^{-4}	3.88×10^{-3} [a]
8	$2H_2 + O_2 + 7Ar$	2.98×10^{2} [b]	6.61×10^{-2}	1.46×10^{-1}	– [c]	– [d]
11	$2H_2 + O_2 + 3.76N_2$ [e]	2.98×10^{2} [b]	1.00×10^{0} [b]	1.50×10^{-2}	1.23×10^{-5}	5.00×10^{-4} [a]
12	$2H_2 + O_2 + 7Ar$	1.20×10^{3}	1.17×10^{0}	1.54×10^{-2}	2.76×10^{-5}	8.14×10^{-5} [f]
13	$2H_2 + O_2 + 7Ar$	1.20×10^{3}	1.17×10^{0}	1.54×10^{-2}	2.76×10^{-5}	3.00×10^{-2}
14	$2H_2 + O_2$	3.00×10^{2}	1.00×10^{0}	5.30×10^{-3}	7.48×10^{-6}	1.00×10^{-2} [a]
15	$2H_2 + O_2 + 3.76N_2$	9.00×10^{2}	2.27×10^{-1}	1.38×10^{-1} [g]	2.23×10^{-4} [g]	1.00×10^{0} [h]

Table 3. Comparison of length scales among various models which use detailed kinetics to describe detonations in hydrogen-based systems. Unless otherwise indicated, parameters are inferred from those reported by the original authors and are for CJ detonations. Values for ℓ_{ind} and ℓ_f were predicted from the algorithm of the present study. [a]Smallest discretization considered. [b]Value not reported, but presumed. [c]Intrinsic low dimensional manifold used, finest scale not obvious. [d]Adaptive mesh refinement method used, grid size not obvious. [e]Presumed stoichiometric; detonation overdriven at $D = 2.065 \times 10^5$ cm. [f]Adaptive mesh refinement method used. [g]Effects of Nitrogen chemistry neglected in estimate. [h]Rough estimate from parameters provided.

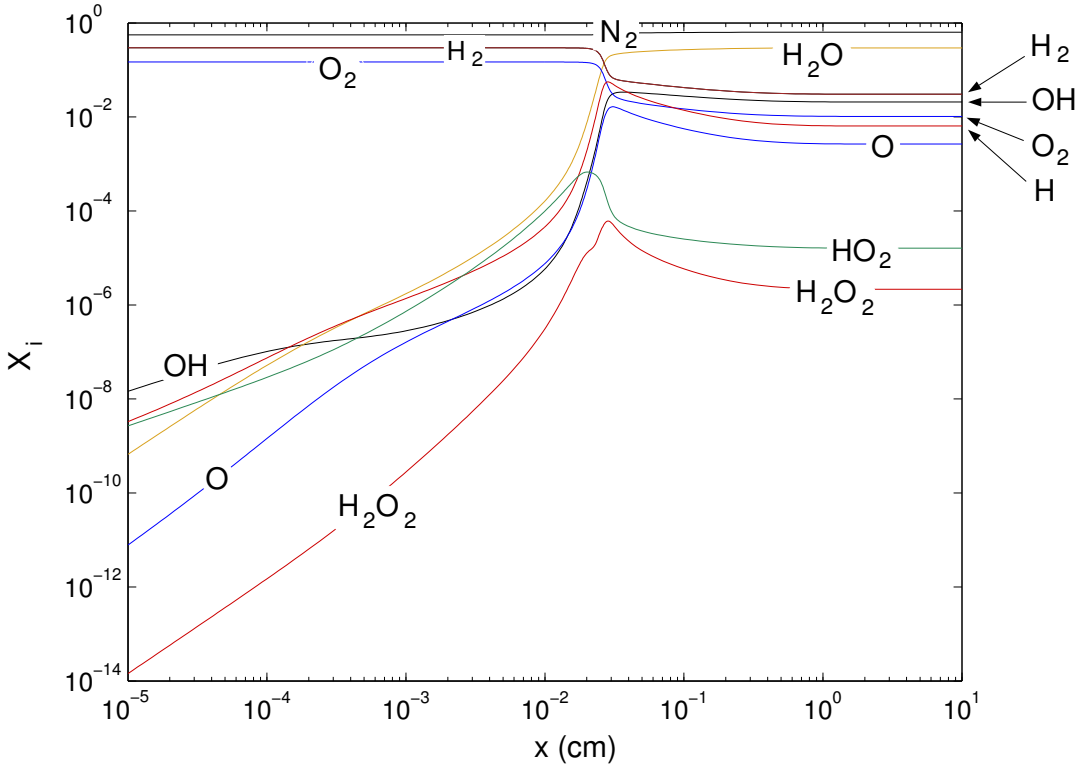

Figure 1. Species mole fraction versus distance.

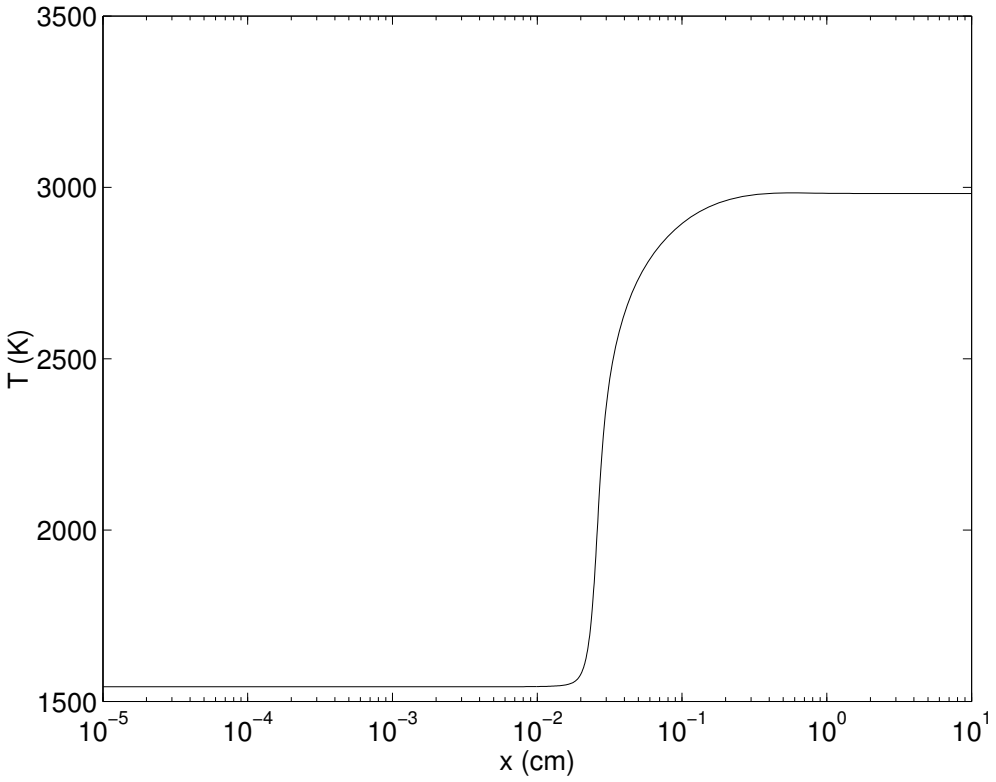

Figure 2. Temperature versus distance.

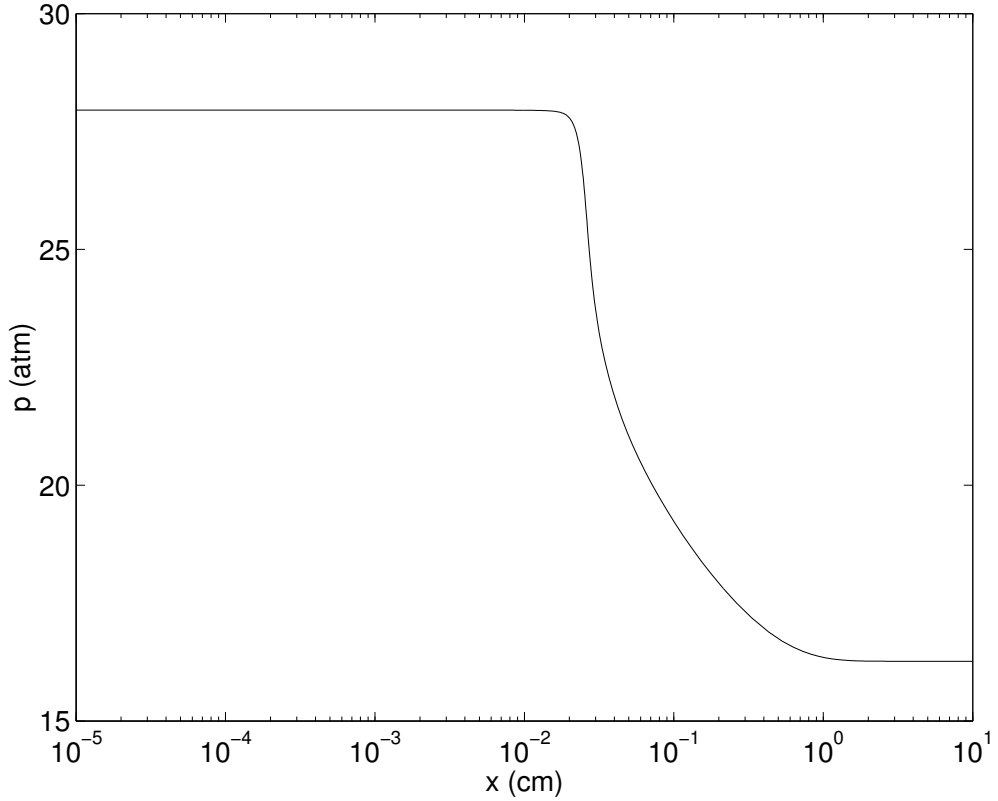

Figure 3. Pressure versus distance.

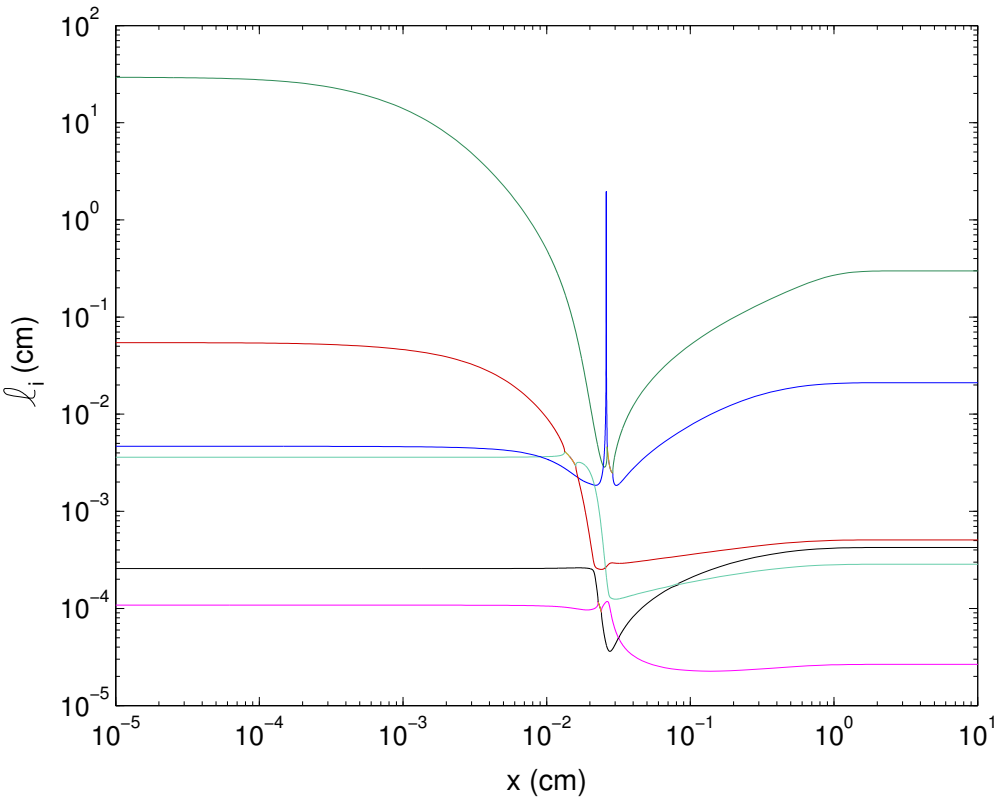

Figure 4. Length scales versus distance.

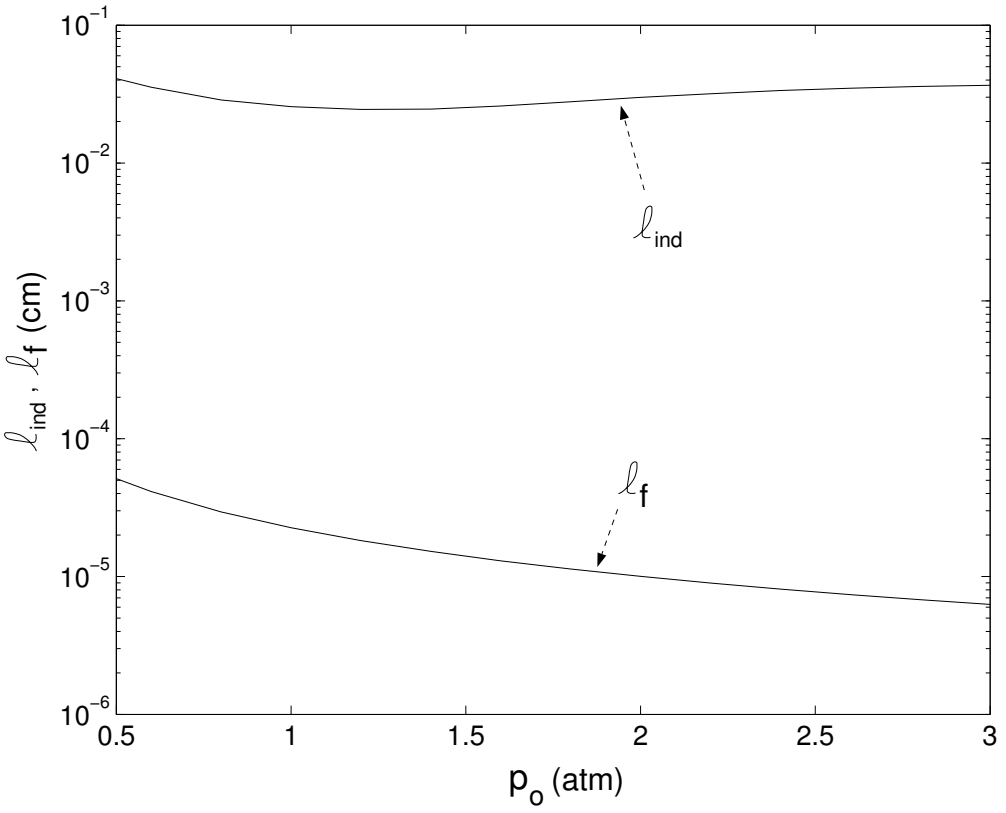

Figure 5. Induction zone length and finest length scale versus initial pressure.

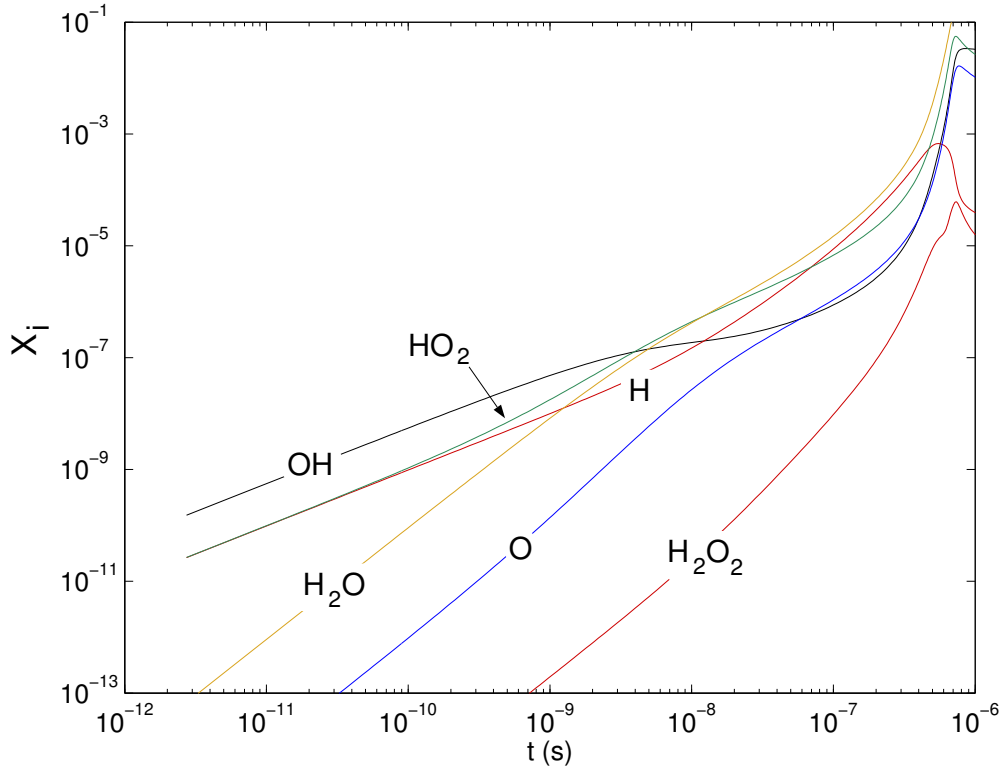

Figure 6. Minor species mole fractions versus time in the induction zone.

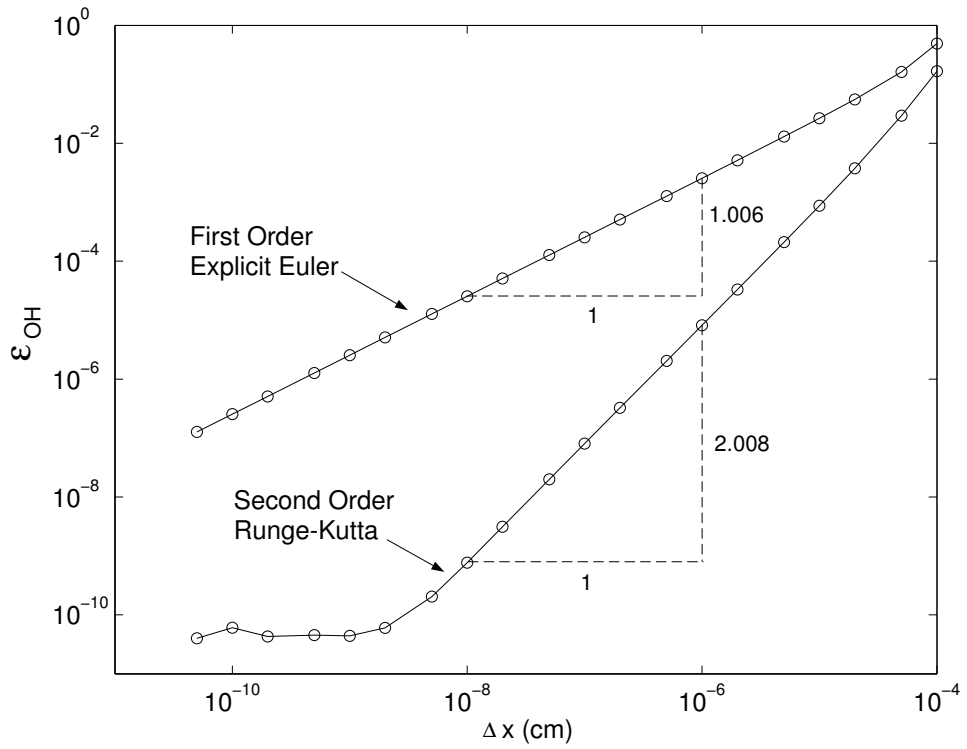

Figure 7. Relative error in X_{OH} at $x = 1 \times 10^{-4}$ cm as a function of discretization scale Δx.

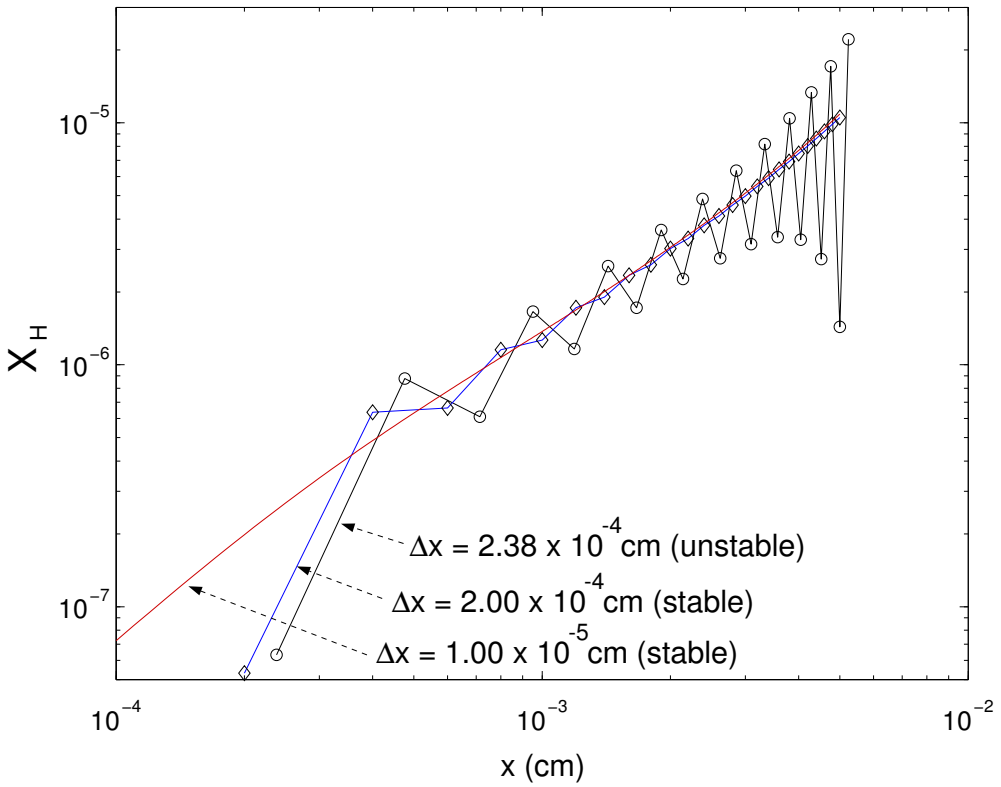

Figure 8. X_H versus x in the near shock region using with a first order explicit Euler method.